Occurrence of Large Geomagnetically Induced Currents Within the EPRI SUNBURST Monitoring Network

Chigomezyo M. Ngwira[1,2,a*], Robert Arritt[3], Charles Perry[3], James M. Weygand[4], and Rishi Sharma[3]

[1]Orion Space Solutions, Louisville, CO, USA
[2]Space Weather Laboratory, NASA Goddard Space Flight Center, MD, USA
[a]Now at Department of Physics, Catholic University of America, Washington DC, USA
[3]Electrical Power Research Institute, CA, USA
[4]Department of Earth, Planetary, and Space Science, UCLA Los Angeles, CA, USA

Key Points:

- We analyze GIC measurements collected under the EPRI SUNBURST project from across the United States and Canada.
- About 76% of the top 17 GIC events occur during main phase of geomagnetic storms, while 24% during sudden storm commencement.
- For the first time it is directly shown that mid-latitude positive bays can cause large GICs at US locations.

*Orion Space Solutions, 282 Century Place, Louisville, CO 80027

Corresponding author: Chigomezyo Ngwira, `chigomezyo.ngwira@nasa.gov` or `ngwirachigo@gmail.com`

Abstract

Space weather, a natural hazard, can adversely impact ~~man-made technological assets~~human technological assets. High-voltage electric power transmission grids constitute one of the most critical technological systems vulnerable to space weather driven geomagnetically induced currents (GICs). One of the major challenges pertaining to the study of GICs over the continental United States has been the availability of GIC measurements, which are critical for validation of geoelectric field and power flow models, for example. In this study, we analyze GIC measurements collected at 17 Electrical Power Research Institute (EPRI) SUNBURST transformer locations across the United States for which a GIC value of 10 A or greater was recorded. This dataset includes 52 individual geomagnetic storms with Kp index 6 and above during the period from 2010 to 2021. The analysis confirms that there is a good correlation between the number of geomagnetic storms per year and the number of recorded GIC events. Our results also show that about 76% of the top 17 GIC events are associated with the storm main phase, while only 24% are attributed to storm sudden commencements. In addition, it is shown, for the first time, that mid-latitude positive bays can cause large GICs over the continental United States. ~~Finally, some GIC events are not well correlated with dB/dt variations, therefore, a more details analysis of individual GIC events is suggested for a better understanding of their production and the coupling of space weather to the power grid.~~Finally, this study shows that the largest measured GIC event in the dataset was associated with a localized intense dB/dt structure, which could be attributed to substorm activity.

Plain Language Summary

Space weather, a natural hazard, can adversely impact ~~man-made technological assets~~human technological assets. High-voltage electric power transmission grids constitute one of the most critical technological systems vulnerable to induced currents produced by enhanced space weather conditions. One of the major challenges pertaining to the study of these induced currents over the continental United States has been the lack of measurements. In this study, we analyze induced current measurements collected at 17 high-voltage power transformer locations across the United States for which a value of 10 A or greater was recorded during the period from 2010 to 2021. The analysis confirms a good correlation between the number of geomagnetic storms per year and the number of recorded induced current events. The results also show that about 76% of the top 17 induced current events are associated with the storm main phase, while only 24% are attributed to storm sudden commencements. In addition, it is shown for the first time that mid-latitude positive bays can cause large induced currents over the continental United States. Finally, this study also shows that the largest measured GIC event in the dataset was associated with a localized intense dB/dt structure, which could be attributed to substorm activity.

1 Introduction

Human technology is vulnerable to space weather, a natural hazard. High-voltage electrical power transmission grids constitute one of the most critical ~~man-made~~human technological systems vulnerable to space weather driven geomagnetically induced currents (GICs) (Pirjola, 2000; Boteler, 2001). Failure of the Hydro-Quebec power grid in Canada during the March 13, 1989 superstorm is a strong reminder of the detrimental impact that GICs can have on power systems (Boteler, 2001, 2019; Bolduc, 2002). But perhaps a less known impact resulting from the March 1989 event is the major equipment damage of two generator step-up transformers at La Grande 4 generating station (North American Electric Reliability Corporation, 1989). ~~The equipment damage was not directly attributed to GICs, but was a result of temporary over-voltage caused by load shedding and~~

~~system separation~~The equipment damage was not directly attributed to GICs, but was a result of temporary over-voltage that caused the loss of static compensators and subsequent line tripping leading to uncontrolled load shedding and system separation. This cascading effect of events was triggered by GICs. Therefore, it is critical that we understand the drivers of GICs, their coupling to the electrical power grid and the system response.

Geomagnetic storms are triggered by the transfer of energy during periods of enhanced solar wind interaction with the Earth's magnetosphere-ionosphere (MI) system, for example during the arrival of a coronal mass ejection (CME). Within the space physics community, understanding the MI coupling processes is regarded as one of the top priority areas of interest. When considering the space weather aspect, special attention is paid to the geomagnetic field fluctuations, which are a good indicator of the GICs. However, many other equally important factors that affect GICs, such as the conductivity of the Earth, configuration of the system, or the type of high-voltage transformer, are usually left out. The scientific importance of the target phenomena in the context of space weather is discussed by (Pulkkinen et al., 2017) and the importance of power grid applications is emphasized by the Federal Regulatory Energy Commission's (Federal Energy Regulatory Commission, 2015) ruling on geomagnetic disturbances (GMDs).

The White House-led National Science and Technology Council identified GICs as a top national threat (National Space Weather Strategy and Action Plan, 2015/2019). Over the last several years, there has been a notable increase in the number of GIC studies in the United States and other countries. These studies include data analysis (Ngwira et al., 2013; Pulkkinen et al., 2015; Dimmock et al., 2020; Schillings et al., 2022), empirical and numerical simulations (Ngwira et al., 2014; Lucas et al., 2020; Welling et al., 2020; EPRI, 2020; Blake et al., 2021), and more recently machine learning techniques have become popular (Keesee et al., 2020; Pinto et al., 2022; Blandin et al., 2022). As well, there are a number of studies that have focused on the engineering aspects of GICs (Horton et al., 2012; Bernabeu, 2013; Overbye et al., 2013; Oyedokun et al., 2020). To a large extent, most of the studies have either focused on the geophysical aspect, which involves space weather and geology or on the engineering component, which requires a knowledge of the power system parameters. This has largely been due to the disconnect between the science and engineering communities. On one hand, it is difficult for the science community to access GIC measurements, and on the other hand, the power utilities are reluctant to share the data due to its sensitive nature.

As a result, one of the major challenges pertaining to the study of GICs, especially over continental United States, has been the availability of GIC measurements. This is critical in the process of validation of geoelectric field and power flow models, for example, which are key for creating mitigation plans. However, it must be emphasized that having the GIC measurements is only one piece of the puzzle because detailed information about the power system is still required for a more accurate determination and interpretation of the GIC impact on the power system. Therefore, a complete analysis of GICs requires a concerted effort that includes the space physics, earth science, and engineering communities.

In this study, we perform an analysis of (1) measured GIC data collected by U.S. and Canadian power utilities under the Electric Power Research Institute (EPRI) SUNBURST project, and (2) the corresponding geomagnetic field information for selected events. The study includes a statistical analysis of recorded GICs above 10 A covering the period from 2010 to 2021 followed by an in-depth examination of the top three largest GIC recordings in the data set. In Section 2 we outline the data sources and highlight the ground geomagnetic stations used for our analysis. The results and their interpretation are discussed in Section 3, while the summary and conclusions are presented in Section 4.

2 Data

2.1 GIC Recordings

The North American Electric Reliability Corporation (NERC) recently (2022) made GIC data publicly available for designated strong geomagnetic storm events with Kp index value of 7 or greater. The data release is in line with the Federal Energy Regulatory Commission (FERC) Order No. 830, which mandates NERC to collect GIC and magnetometer data to support ongoing research and analysis of GMD risk. This data is available to the public and can be accessed through the NERC GMD website. However, it is important to understand that simply knowing the value of GIC is not enough to deduce the impact on a power system. The power grid response to GMD conditions is a complex, multi-dimensional issue (Gritsutenko et al., 2023). A number of important factors that affect GICs, such as the conductivity of the Earth, configuration of the transmission network to determine system resistance and orientation to the electric fields, or the type of high-voltage transformer where specific design details (e.g. core type, voltage level, winding construction, etc.) are needed to be known to determine a transformer's unique response to GICs; however, due to critical energy infrastructure concerns – the latter two parameters are not available without specific agreements with the power utilities. For a better understanding of the data required to make a proper impact assessment, readers are encouraged to consult Moodley and Gaunt (2017) and Lewis et al. (2022).

The data presented in this study comprises of GIC measurements recorded at ~~1~~7 EPRI SUNBURST transformer locations across the United States and southern Canada. The SUNBURST project is a collaborative GIC monitoring effort (Lesher et al., 1994; EPRI, 2008), which also includes their impact on the electric power grid. Utility members collectively fund the project network, which consists of about 50 monitors on transformer neutrals across North America. The monitoring effort helps to better inform utilities with respect to GIC flows on their transmission system, validation of GIC models, and assessment of vulnerability. EPRI performs periodic upgrades of its monitoring sensors to bring the hardware up to date and to reduce costs by adopting off-the-shelf components with customized software. The latest updates on the SUNBURST can be viewed on the website (`www.sunburstproject.net`). Readers must note that the EPRI SUNBURST data is not directly available to the public, however, since it is also part of the larger NERC dataset, it can be accessed through the NERC website, as well.

Table 1. List of geomagnetic Observatories locations used in the analysis of the ground geomagnetic field response. The locations are give in ~~geographic coordinates~~geographic and geomagnetic coordinates.

Name	Code	Operator	Latitude Deg.	Longitude Deg.	MLAT Deg.	MLON Deg.
Boulder	BOU	USGS	40.14	254.76	48.52	-38.69
Stennis Space Center	BSL	USGS	30.35	270.36	40.69	-17.89
Federicksburg	FRD	USGS	38.21	282.63	48.05	-0.64
Fresno	FRN	USGS	37.09	240.28	42.63	-54.89
New Port	NEW	USGS	48.27	242.88	54.65	-54.82
Ottawa	OTT	NRCan	45.40	284.44	54.98	2.52
Tucson	TUC	USGS	32.17	249.27	39.32	-43.96
Pinawa	PIN	CARISMA	50.20	263.96	59.96	-27.43

EPRI SUNBURST monitoring devices are installed at some substations to obtain vital information about the characteristics of GICs. The sensors detect the presence of DC (direct currents) on the transformer neutral at a sampling rate of 1-2 seconds but most have been upgraded to 1-second now. The data output from the sensors is routed via a Supervisory control and data acquisition (SCADA) system. Ideally, sensor are designed to measure currents in the range of 1000 A, while the range of frequency is between 0.01–0.0001 Hz. ~~The data covers the period~~The data presented in this paper covers the period from 2010 to 2021 and is limited to events for which GIC values greater than 10 A were recorded. After applying this selection criteria, only 17 transformer locations were available for our analysis. This is because some sites are more active than others due to geological location, earth conductivity, voltage level, transmission line orientation, etc. In general, the stations are concentrated around central and eastern United States and southern Canada. Based on this event selection criterion, geomagnetic storms with a recorded Kp of 6, which are not in the the NERC data set, are also included in the analysis. Though the Kp index is not a good indicator of GICs, it is used in the present study only in terms of classifying the level of geomagnetic activity associated with each GIC event.

2.2 Geomagnetic and Geoelectric Fields

For interpretation of geomagnetic field response, we use ground magnetometer recordings obtained at the USGS chain of observatory stations in the United States and ~~the NRCan Ottawa observatory site~~some magnetometer sites in Canada. The list of these magnetometer sites is displayed in Table 1. The magnetometer data is used in this study to investigate geomagnetic variations during each of the storm events that have been identified. We have analyzed the geomagnetic field rate of change dB/dt during each storm event and at each ground magnetometer in Table 1 to get a sense of the overall geomagnetic field characteristic response across the entire United States. Here, $\mathrm{B}_h = \sqrt{Bx^2 + By^2}$ from which we then compute dB/dt as dB_h/dt using 1-second and 60-second samples of the geomagnetic field data. For the induced geoelectric fields, we used the EPRI geoelectric field computational tool that ingests geomagnetic fields and ground conductivity information (EPRI, 2022). The geoelectric field is computed at the resolution of the geomagnetic field data, which is 1-second for the current study. The current version of the tool is configured to take into account the 3D nature of the Earth's surface through use of magnetotelluric transfer functions (Kelbert et al., 2011, 2017). For more detailed discussions concerning transfer functions, interested readers should refer to Schultz (2009) and Kelbert (2020).

3 Results and Discussions

~~In this section, a statistical analysis is presented followed by a close examination of the three most significant GICs in the recorded data set.~~ In this section, a statistical analysis is presented followed by a close examination of three large GIC events that depict different driving characteristics.

3.1 Statistical Overview

As mentioned earlier, ~~this study hinges on GIC recordings taken from across the United States~~this study hinges on the EPRI SUNBURST project GIC recordings from across the United States and southern Canada covering the period from 2010 to 2021. The histogram in Figure 1 displays a collection of measured GIC events that meet the selection criterion outlined above for all the 17 SUNBURST locations. As seen, the distribution shows that there are more events captured with GIC less than 25 A. Not surprising, very few large amplitude GICs (> 30 A) have been observed during the period of study. It is important to note that there have been very few intense geomagnetic storms observed during solar cycle 24 compared to the previous three cycles. For example, there are about 24 individual storms with Kp 7 or greater in our data set (2010-2021) with very few reaching Kp level 9, while there were more than 40 individuals storms with similar Kp in the period 2000-2005 including many with Kp level 9. Given that, it is expected that more higher amplitude GICs may be observed for relatively more active solar cycles, such as cycle 22 or 23.

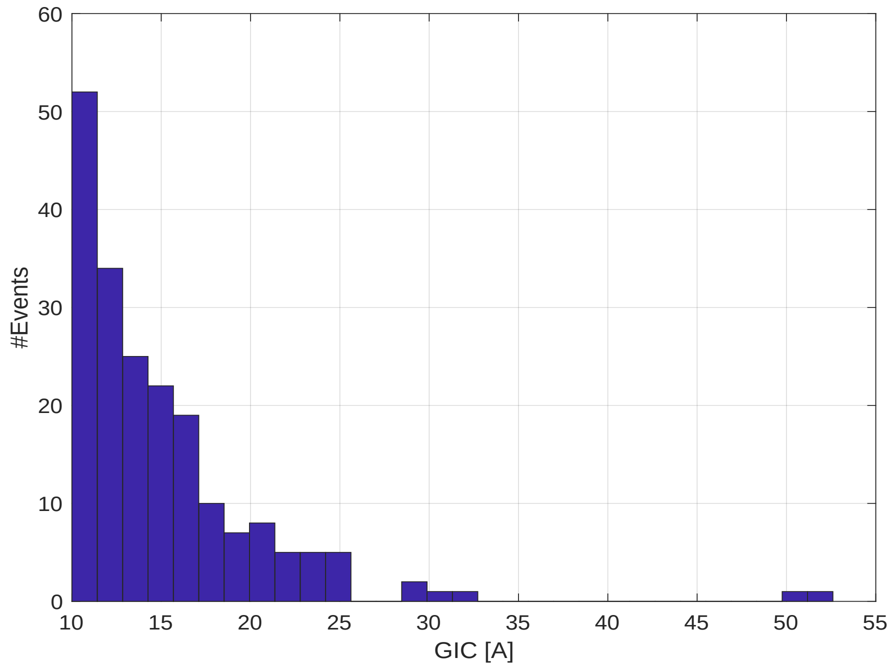

Figure 1. Distribution of measured GIC events with current above 10 A during the period from 2010 to 2021. The data was collected at 17 EPRI SUNBURST nodes across the United States.

It is well-known that the number of large GIC events is closely correlated to the occurrence of GMDs. However, it is not the magnitude of the storm that defines the level of GICs but the induced geoelectric field, which is determined by a combination of geomagnetic variations, dB/dt, and the ground conductivity. Exhibited in Figure 2 is a summary of GIC events (blue) and GMDs (red) for the period 2010 to 2021. Clearly, there is a good correlation between the number of recorded GIC events in each year and the number of geomagnetic storms with Kp > 6, as expected. On closer inspection, 2012 and 2015 have relatively similar number of storms, but the number of GIC events is vastly different. There are about twice as many recorded GIC events in 2015 compared to 2012. The most likely source of this difference is that there were fewer number of GIC sites available in 2012 compared to 2015, as the number of SUNBURST nodes keep increasing. There were only ten GIC monitors available to this study in 2012 compared to the sixteen available by 2015. However, EPRI had a total of 13 installed monitors in 2012 and 30 plus by 2015. On the other hand, this does not fully explain why more recorded GICs are seen in 2012 than in 2016, 2017 and later years. ~~It is possible that there exists some factors that could be related to the geoeffectiveness of the disturbances that may lead to an increased number of observations in 2015~~It is possible that there exists some factors that could be related to the characteristics of the disturbances leading to an increased number of observations in 2015. In addition, it is evident in Figure 2 that more geomagnetic storms with Kp > 6 were observed in 2012 than in 2016 or 2017.

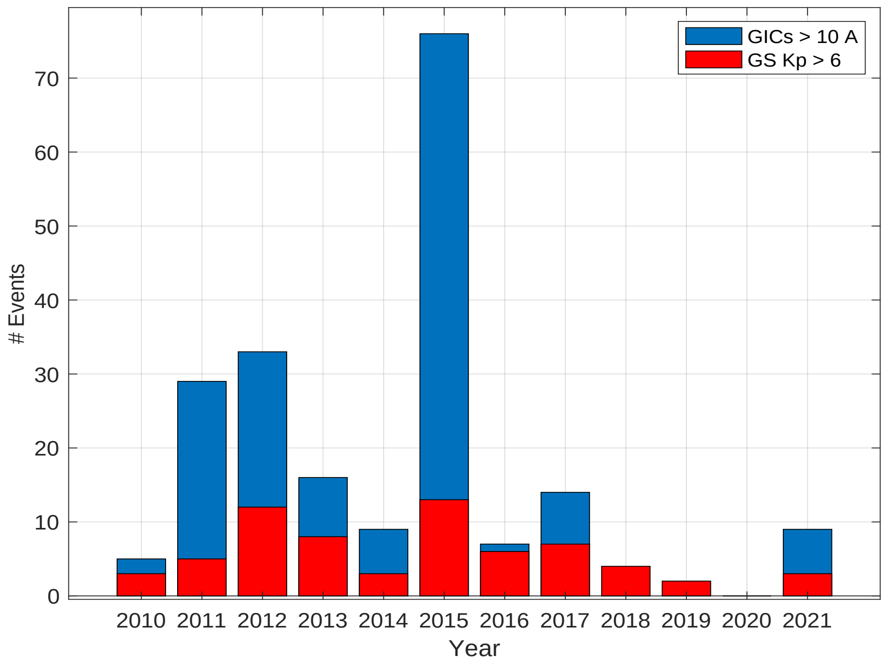

Figure 2. Summary of measured GIC events (blue) with current above 10 A across the United States during the period from 2010 to 2021. The red bars indicate the number of geomagnetic storms (GS) with Kp index greater than 6 for each given year, respectively.

Next we examine the maximum recorded GIC values at each of the GIC nodes listed in Table 2. Unfortunately, the actual names of the sites have been withheld due to the sensitive nature of the information. Nevertheless, Table 2 provides information concerning the recorded GICs including the date, site number, the maximum recorded GIC, the time of maximum GIC, maximum Kp index, and the phase of the storm during which the maximum GIC was observedsite number, the maximum recorded GIC, date maximum GIC was recorded, the time of maximum GIC, the phase of the storm during which the maximum GIC was observed, and the minimum Dst index value during the respective GMD event. Here, we used the Sym-H index, a high-resolution (1-minute) equivalent of the hourly Dst index, to determine the phase of the storm when the GIC measurements were recorded according to definitions outlined by (Akasofu, 2018).

It is worth noting that Sites #4 and #5, as well as Sites #9 and #10 are two different transformers located at the same substation. The difference in level of GICs at these locations highlights the complex nature of GIC response, especially at #9 and #10 where the difference is slightly bigger. However, the details pertaining to the cause of these differences are out of the scope of this paper.Typically, a transformer's response will include nonlinear and frequency-dependant effects, while the flux pattern and winding inductances distributions are unique across all transformer core structures. (Oyedokun, 2015; Rezaei-Zare et al., 2016). The flow of GICs through a transformer is dependant on the system topology, line/grounding resistance, geographic orientation, transformer type, winding resistances, series line compensation, and the geoelectric field (Bernabeu, 2013). In addition, Oyedokun (2015) demonstrated that the transformer response time, which takes into account the size and core type, is also a critical parameter when assessing the transformer response to GICs.

Table 2. Summary of the top 17 measured GIC events at different nodes across the SUNBURST network during the period from 2010 to 2021. The table also includes the associated geomagnetic storm information.The table also includes the associated GMD event phase and the minimum Dst value associated with each GMD event. The symbols represent: SSC - Sudden storm commencement and MP- Main phase.

Location	Max GIC [A]	Date of Max GIC	Time of max GIC UT/LT [hh:mm]	Storm phase	GMD strength Min. Dst [nT]
Site #1	24.7	26/09/2011	19:36/14:36	MP	−118
Site #2	25.2	24/10/2011	18:31/13:31	SSC	−147
Site #3	23.7	23/06/2015	03:32/22:32	MP	−198
Site #4	52.6	09/09/2015	11:01/06:01	MP	−105
Site #5	50.1	09/09/2015	11:01/06:01	MP	−105
Site #6	22.2	23/06/2015	03:32/22:32	MP	−193
Site #7	30.8	26/09/2011	19:37/14:37	MP	−118
Site #8	17.8	08/09/2017	01:34/20:34	MP	−128
Site #9	11.3	12/09/2014	15:54/10:54	SSC	−88
Site #10	20.0	12/09/2014	15:54/10:54	SSC	−88
Site #11	15.9	12/05/2021	12:20/07:20	MP	−60
Site #12	12.1	22/06/2015	18:33/13:33	SSC	−198
Site #13	20.2	12/09/2014	22:54/17:54	MP	−88
Site #14	31.9	02/10/2013	04:34/23:34	MP	−72
Site #15	11.6	17/03/2015	13:50/08:50	MP	−234
Site #16	18.7	22/06/2015	20:04/15:04	MP	−198
Site #17	10.3	12/05/2021	12:19/07:19	MP	−60

Looking back at Table 2, the maximum recorded GIC for the entire period of study occurred at Site #4 on 09/09/2015. This GIC measurement was associated with the main phase (MP) of a geomagnetic storm that reached Kp index value of 6 and is further discussed in Section 3.4. Also noteworthy is that most (76%) of the 17 incidences listed in Table 2 occurred during the main phase of geomagnetic storms, while a few (24%) are associated with sudden storm commencement (SSC). We must caution the readers that these percentages specifically pertain to the GIC events in Table 2 and may not be valid for the entire dataset. Furthermore, majority of eventsthe majority of GIC events (13 out of 17) are observed during the local daytime with few events during the local nighttime, as illustrated in Table 2. Since most of the United States power grid is located in the higher mid-latitudes to the low-latitudes, the absence of events around local midnight indicates that auroral substorms are not likely to be a driving source. However, it should be noted that auroral activity can sometimes produce large GICs in mid-low latitudes during extreme geomagnetic storms as the auroral current can extended into those regions (Ngwira et al., 2013, 2015; Weygand et al., 2023). Case study #2 in the present paper highlights one of such cases of auroral activity driving GICs at mid-latitudes.

Furthermore, we analyze the geomagnetic conditions across the United States for all individual events listed in Table 2. In particular, we determine the rate-of-change of the horizontal geomagnetic field (combination of Bx/By) and investigate the fluctuations within a ±5 minutes window centered on the time of the maximum recorded GIC at each of the sites listed in Table 1. The results of this investigation are presented in Table 3. Interestingly, the geomagnetic rate-of-change values on 09/09/2015 are the lowest for all events. A careful analysis of the GIC events was made and we are very certain that the recorded GIC data was real. This event is further discussed in Section 3.4.Furthermore, we analyze the occurrence of GICs at each individual site. The results are displayed in Table 3 including the total number of observed events at each site, the

Table 3. List of the 17 GIC sites including the total number of observed events at each site during the period from 2010 to 2021, the years the site as been in operation, and the normalized value of the number of events at each site per year.

Location	Total number of events	Years in operation	Events per year
Site #1	11	11	0.82
Site #2	20	11	1.82
Site #3	28	11	2.55
Site #4	29	11	2.64
Site #5	26	11	2.36
Site #6	24	11	2.18
Site #7	11	11	1.00
Site #8	3	8	0.38
Site #9	1	9	0.11
Site #10	4	7	0.57
Site #11	3	10	0.30
Site #12	1	10	0.10
Site #13	2	9	0.22
Site #14	28	10	2.80
Site #15	5	8	0.63
Site #16	3	7	0.43
Site #17	1	1	1.00

time the site as been in operation, and the normalized value of the number of events at each site per year. The normalization takes into account that the monitoring sites were not installed during the same period. For instance Site #7 and Site #17 have the same number of events per year but the number of observed events was different. There was one event observed at Site #17 which was in operation for only one year at the time compared to the eleven events observed at Site #7 during its eleven years of operation. Clearly some sites have a higher occurrence of GICs than others. This could be caused by several factors, such the location of the site in latitude, the node location with respect to the grid configuration, transformer design, or the local geoelectric field at the site, as discussed earlier above. However, a higher occurrence of GICs does not necessarily mean a higher risk of failure of that transformer. Some transformer designs allow for large GIC flows, while others may not. In order to ascertain the risk of each transformer, it would require separate detailed analyses, as discussed earlier.

3.2 Case Study #1 - Event on 24/10/2011

Earlier studies have established that the dynamic interaction of the dayside magnetopause with solar transient features can cause a variety of the magnetospheric perturbations at various scales (Oliveira & Raeder, 2014; Yue et al., 2010). It is well-known that when the enhanced solar wind pressure suddenly compresses the dayside magnetopause, a large step-function-like increase of the geomagnetic field intensity observed by ground-based magnetometers is produced (Villante & Piersanti, 2011; Yue et al., 2010). This is commonly referred to as the storm sudden commencement (SSC) or sudden impulse (SI) (Kikuchi & Araki, 1979). Large impulsive geomagnetic field variations from SSC are well understood to be a concern for power grids (Kappenman, 2003).

The GIC event on 24 October 2011 was clearly triggered by a SSC at the time of a CME arrival. Solar wind parameters, geomagnetic field Sym-H index, dB/dt, and GIC variations for this event are presented in Figure 3Solar wind parameters and IMF, the geomagnetic

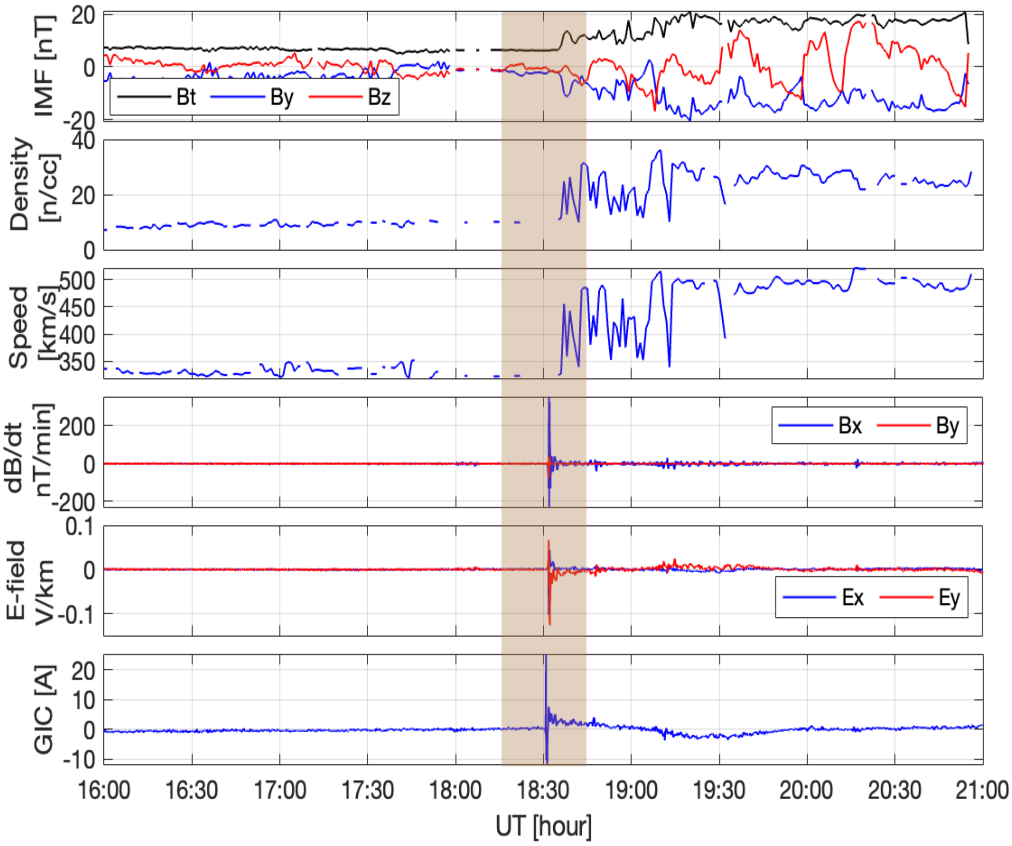

Figure 3. Solar wind, geomagnetic activity, and GIC response during the arrival of a CME on 24/10/2011. The panels display the IMF Bt/Bx/Bz, solar wind density, the solar wind speed, the geomagnetic dB/dt at FRN, the E-field at GIC site and the recorded GIC at Site #2.

dB/dt at FRN, the E-field at GIC site and the GIC variations for this event are presented in Figure 3. Note that the in situ solar wind data not properly aligning with ground observations is a result of the shifting applied on the OMNI dataset. The location of the transformer site from FRN magnetometer site is within 320 miles or 508 km. Evidently, the geomagnetic response, i.e., Sym-H (see supplementary data) and dB/dt, is well correlated with the sudden jump in solar wind flow speed, density, and the IMF total magnetic field, Bt, around 18:31 UT or 14:31 PM local time on the east coast of the United States. The Bt abruptly increased from about 6 nT to around 13 nT, the speed jumped from 320 km/s to 450 km/s, while the density increased from roughly 10 n/cc to 25 n/cc at the time of the arrival. The IMF Bz was southward (∼–8.0 nT) at that time then quickly reversed to northward direction. Additionally, Ngwira et al. (2023) reveals that the ~~AE~~auroral electrojet (AE) index also responded with a sudden rapid increase immediately after the CME arrival, which indicates that the CME arrival may have ~~triggered some~~enhanced auroral activity or triggered a substorm (Oliveira et al., 2021).

The sudden increase of solar wind dynamic pressure associated with the solar wind transient structures like interplanetary shocks can produce impulsive geomagnetic responses (Tsurutani et al., 2011; Oliveira et al., 2018; Smith et al., 2019). According to Akasofu (2018), the present understanding of SSCs is that when a CME arrives, the Chapman-

Ferraro current is enhanced, and its magnetic field is manifested as SSC. The Chapman-Ferraro current flows along the magnetopause and separates the Earth's geomagnetic field from the IMF in the magnetosheath. Some studies show that interplanetary shocks can trigger supersubstorms (Tsurutani & Hajra, 2023), which cause very intense geomagnetic variations with an SML less than -2500 nT. The SuperMag SML index is a generalized version of the auroral lower (AL) index used for the identification of substorms (Newell & Gjerloev, 2011). Now, the geomagnetic response during SSC events depends on several factors including the orientation of the CME with respect to the Earth's magnetosphere configuration. Oliveira et al. (2018) studied the impact of interplanetary shocks on the surface geomagnetic field response and revealed that nearly frontal shocks (head-on) were linked with intense geomagnetic perturbations compared to inclined shocks. More recently, Oliveira et al. (2021) show that in comparison to inclined shocks (high tilt), the nearly frontal shocks generate intense nightside substorm energetic particle injections with fast and clear auroral poleward expansion. Furthermore, Oliveira et al. (2021) also found that even though the field-aligned currents associated with both frontal and included shocks were nearly similar in strength, the current variations produced by frontal shocks were larger and faster, thus resulted in more intense dB/dt variations on the ground.

3.3 Case Study #2 - Event on 02/10/2013

On 2 October 2013, shortly before 02:00 UT, a CME was detected at L1 point, as manifested by the sudden intensification of the ~~Sym-H index~~IMF Bt in Figure 4. The shock arrival is not so clear in the solar wind speed and density due to missing data, but the IMF Bt experienced a sudden increase at the time of the arrival. The CME arrival triggered a substorm, as seen by the AE index response (see Figure 5), while a strong rapid geomagnetic field response was observed for dB/dt. Soon after 02:00 UT, the geomagnetic storm main phase started to intensify as noted ~~in the Sym-H index~~through the geomagnetic field Bx component in Figure 5.

Figure 4 indicates that at about 04:18 UT, a sudden jump in Bt and solar wind density was observed. This is consistent with observed Sym-H index (Ngwira et al., 2023), which also shows a slight enhancement around the same time. Then about 16 minutes later at around 04:34 UT, sudden changes in dB/dt, the E-field, and the GIC were observed. This is marked by the brown shaded region in Figure 4. The large GIC value of 31.9 A was recorded at this time. A check of the SuperMag SML index for this event also shows an abrupt rapid decrease ~~at this same instance~~from -120 nT at 04:33 UT to about -640 nT at 04:36 UT, which could be indicative of substorm activity. The dB/dt, E-field, and GIC fluctuations are well correlated during this period of interest.

We propose that the large GIC event observed on this day was linked to the mid-latitude positive bay (MPB), a phenomenon that is driven by auroral substorm-related activity (Chu et al., 2015; McPherron & Chu, 2017). Furthermore, we postulate that the substorm may have been triggered by the sudden large density enhancement prior to the MPB event. This is supported by the observed MPB seen in the detrended geomagnetic field horizontal component Bx in Figure 5. The MPB is highlighted in the brown shaded area. The average value of Bx ~~before the storm was~~within a 2-3 hour quite-time window before the SSC was used in the detrending process to remove the background variations. Clearly, all the mid-latitude magnetometers in the United States responded similarly, including the magnetometer at OTT which is more of a higher mid-latitude location.

Previous studies have shown that MPBs are a prominent feature at mid-latitudes during substorm events (Chu et al., 2015; Guerrero et al., 2017; McPherron & Chu, 2018). McPherron and Chu (2018) explain that a westward current moves through the expanding aurora at the onset of the substorm expansion phase. This current is a manifestation of the substorm current wedge (SCW) created by the diversion of the tail current along magnetic field lines. ~~In Figure 6 we present the spherical elementary currents (SECs) derived from ground-based magnetometer chains in North America and Greenland~~ (Weygand et al., 2011, 2012). ~~The SECS technique has been widely applied in the study of GMDs~~ (Weygand et al., 2016; Ngwira et al., 2018; Engebretson et al., 2021; Oliveira et al., 2021). ~~As seen in Figure 6, both the auroral eastward electrojet current (arrows) and the field-aligned currents (color) progressively become stronger during the specific interval of time associated with the GIC event in Figure 4.~~ Nishimura et al. (2020) explain that at low and mid- latitudes, the field aligned currents appear as a rise and decay in the Bx component, which is the MPB, while a negative bay is observed at high-latitudes. Using optical data on board the IMAGE mission, Chu et al. (2015) determined that MPB onsets were in close agreement with auroral onsets and that the MPB signatures were independent of the position of ground stations relative to the ionospheric currents. Therefore, as presented in Figures 4 and 5, the mid-latitude GIC event on 2 October 2013, was most likely driven by substorm-related activity, which is consistent with the presence of a strong MPB observed at US magnetometer locations. To our knowledge, this is the first time that an MPB signature

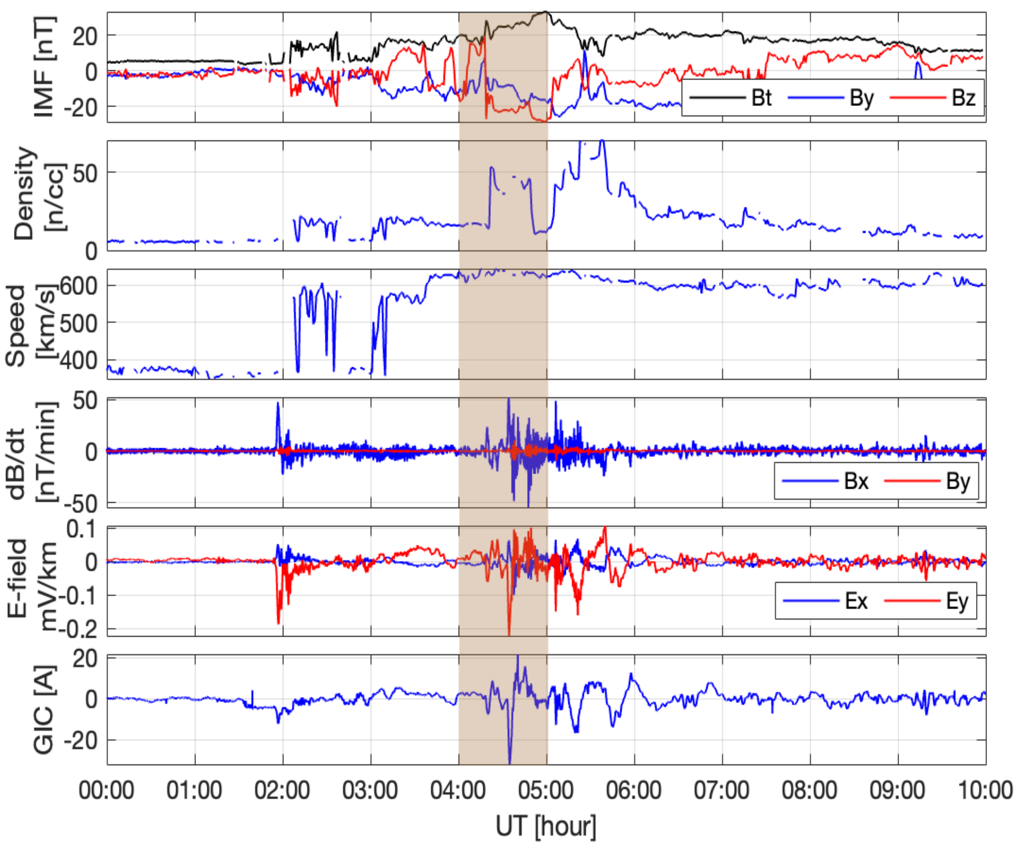

Figure 4. A response of the geomagnetic field and GICs during the CME on 02/10/2013. The top three panels display the IMF Bt, solar wind speed, and density, while the bottom three panels show the dB/dt at FRN, the E-field at GIC node, and the recorded GIC. The GIC Site #14 is within 150 km from FRN. The brown shaded region marks the period around the GIC event.

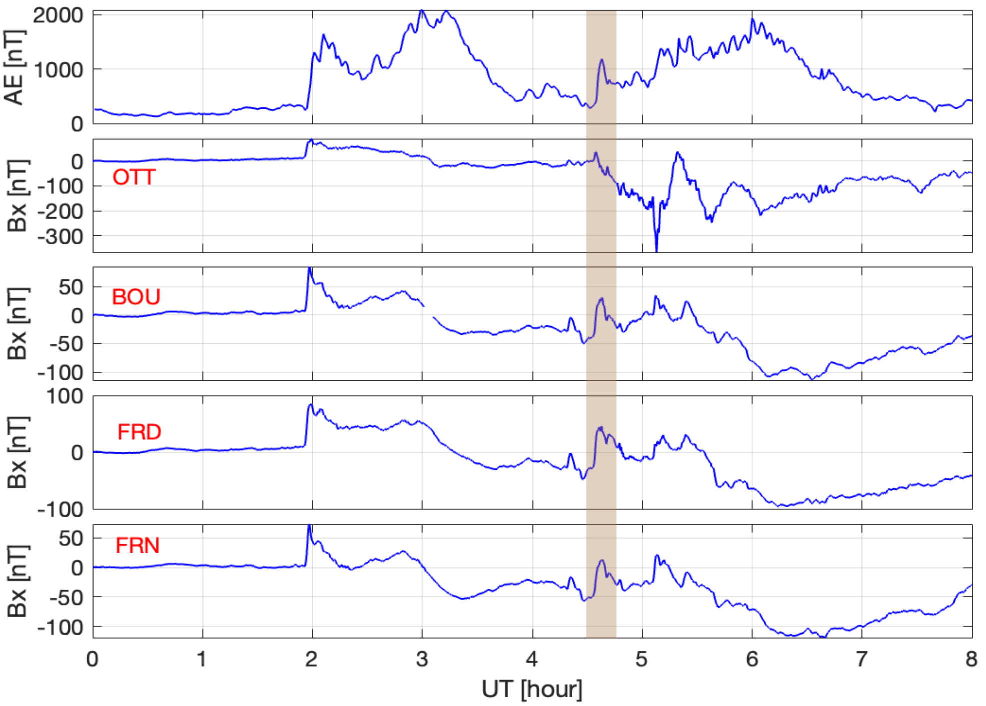

Figure 5. Geomagnetic field response during the GMD event on 02/10/2013. The panels show the AE index and the geomagnetic field Bx component at OTT, BOU, FRD, and FRN, respectively. The response in the brown shaded region highlights the MPB event.

has been directly linked to the generation of large GICs recorded on a high-voltage power transformer.

3.4 Case Study #3 - Event on 09/09/2015

This event has the largest currents from our list of events in Table 2. GIC values of 52.6 A and 50.1 A were measured at 11:01 UT corresponding to 07:01 AM local time on the east coast of the United States. Although these GIC events were recorded around the peak of the main phase of a geomagnetic storm with Sym-H index around -100 nT, the dB/dt values determined at USGS observatory sites in United States were notably low in comparison to other events, as exhibited in Table 3 and further demonstrated in Figure 7. The vertical dashed grey line under the shaded area in this figure denotes the time of the maximum GIC. There are some notable changes in the IMF By component, the solar wind density decrease, and enhancement of SML index from -815 nT at 10:59 UT to -1073 nT at 11:03 UT. However, a closer inspection of dB/dt results from all the ground magnetometers shows similar characteristics as in Figure 6 where very small variations were present at 11:01 UT.These GIC events were recorded around the peak of the main phase of a geomagnetic storm with Sym-H index around -110 nT. The IMF, solar wind, the dB/dt, and GIC values are displayed in Figure 6. The shaded area denotes the period of interest. Some notable changes in Figure 6 around 11:00 UT include a sudden decrease of the IMF By component, the solar wind density decrease, and enhancement of SML index. These changes also correspond to the changes in dB/dt for the ground magnetometer at Pinawa in southern Canada and the large GICs observed at Site #4 and #5. Unfortunately, there was no ground conductivity information for the GIC site, therefore, the electric fields were not computed for this specific case.

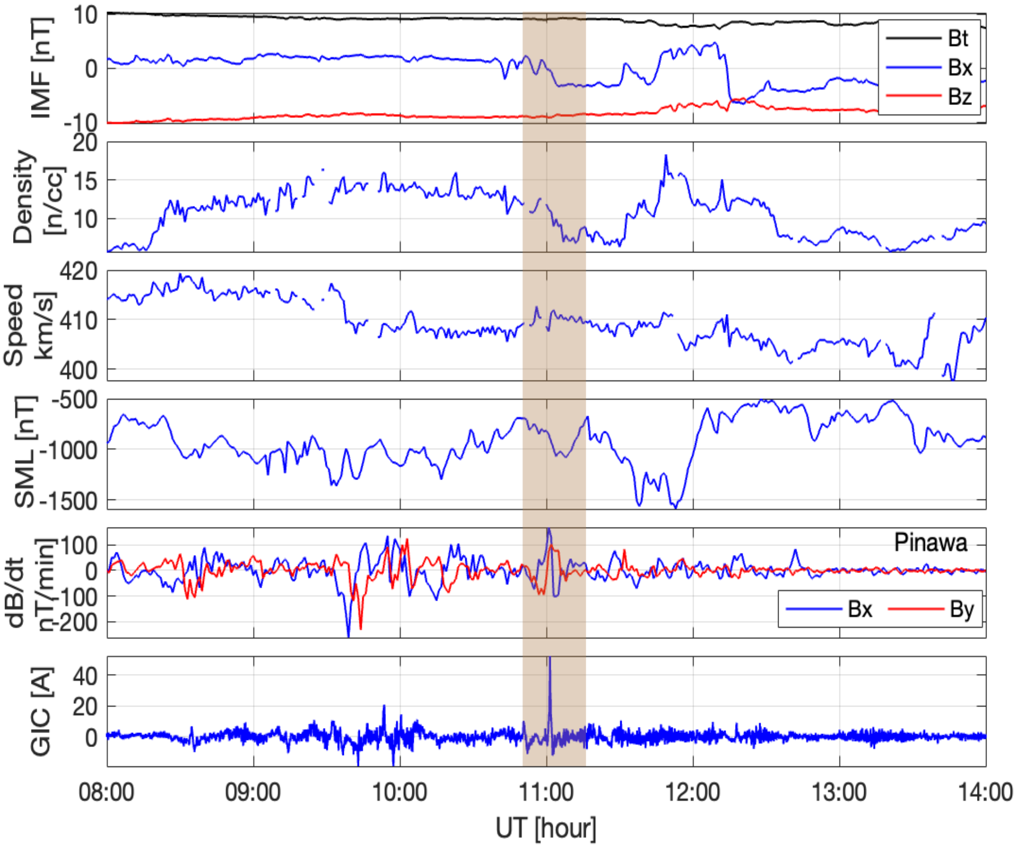

Figure 6. Characteristic response of IMF, solar wind density, SML index, Sym-H index, geomagnetic dB/dt, and the GICs during the geomagnetic storm on 09/09/2015. ~~The vertical grey line under the shaded area indicates the time of the maximum GIC recorded at Site #4 in Table 2.~~The shaded area represents the time of the maximum GIC recorded at Site #4, which is located in the southern region of Canada near the United States border. We computed dB/dt from the magnetometer data at Pinawa in Canada, which is a little over 400 km from the GIC site.

~~If this event was space weather driven, we would expect to see a large corresponding change in dB/dt at the time of the GIC event. So, are these GIC values real or are they caused by other non space weather drivers? A closer examination of the raw GIC data reveals that the measurements appear to be legitimate. Therefore, because of the fact that the peak GIC is not well correlated with large dB/dt variations, we can not ascertain that this event is truly GMD related. Perhaps it could as well be related to a nearby switching event or disturbance at or near the substation. This requires a more detailed analysis that calls for additional observations than available to the authors, thus, it is outside the scope of this paper. Therefore, it is important for the community to note and take caution of such cases when using the publicly available data set. Furthermore, we encourage members of the science community that want to use this data to consult with power utilities or EPRI when using the data.~~

To examine the likely drivers of the large GIC events at Site #4 and #5, we look at the geospace environmental conditions. Specifically, the equivalent ionospheric currents (EIC) and current amplitudes produced by the spherical elementary current system (SECS) approach are employed (Amm, 1997; Weygand et al., 2011). The SECS technique has been widely applied in the study of GMDs (Weygand et al., 2016; Ngwira et al., 2018; Engebretson et al., 2021; Oliveira et al., 2021). The current version of SECS ingests 10-seconds magnetometer data from ground networks across North America and Greenland but can be run at other resolutions (Weygand et al., 2023). Maps of dB/dt distribution pattern computed from the SECS interpolated magnetic field are presented in Figure 7 (left) at three different time steps. The EICs and current amplitudes are presented on the right of this figure. A highly localized intense dB/dt structure is seen around the Pinawa geomagnetic site in the middle panel at roughly 11:00 UT, which is consistent with dB/dt and GIC observations in Figure 6. The localized geomagnetic response feature has been a subject of increasing interest from both the science standpoint and its engineering applications (Ngwira et al., 2015; Engebretson et al., 2021). From the science perspective, one of the major challenges is understanding the magnetosphere-ionosphere processes that drive these localized enhancements

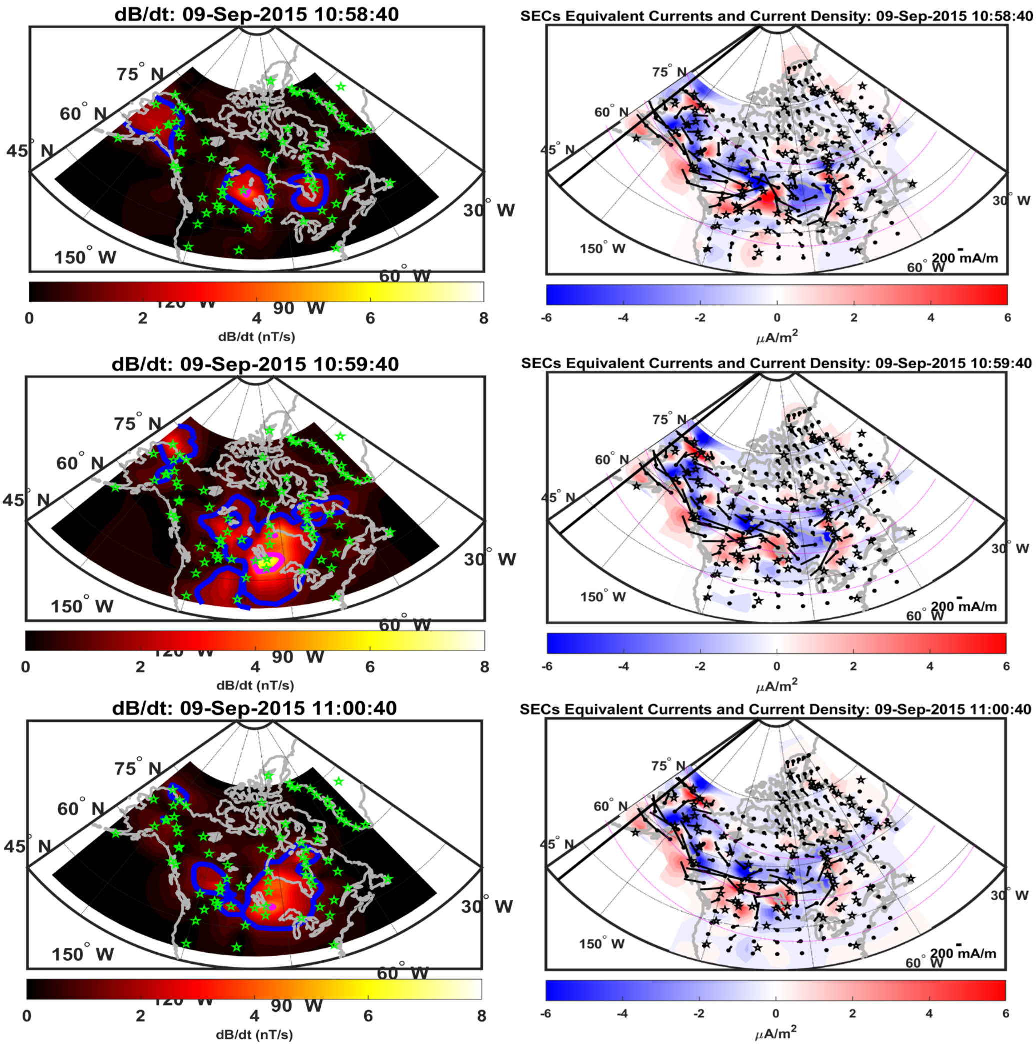

Figure 7. Maps of dB/dt distribution produced from interpolated magnetic fields using SECS techniques following the GMD event 02/10/2013. The images indicate presence of an intense localized dB/dt structure (yellow area) near Pinawa geomagnetic station in southern Canada. The black solid line denotes geographic midnight. The geographic coordinate system is used.

or "hot spots" (Pulkkinen et al., 2017). A further survey of the geomagnetic field perturbations near the United States and Canadian border reveals the presence of strong perturbations particularly in the central to western region of Canada.

The current patterns in Figure 7 (right) show a predominately westward current (arrows) exiting over the southern parts of Canada. The location of this current system along the United States and Canadian border suggests that the auroral oval expanded significantly from its quiet-time location, which is usually in the northern parts of Canada. Typically, auroral expansion is usually associated with the strengthening of the SCW (Kepko et al., 2015; McPherron & Chu, 2017). At about 11:00 UT, IMF Bz had been predominately southward for about 9-hours while the Dst index was roughly -110 nT, which resulted in strong geomagnetic conditions and expansion of the auroral oval. As seen in Figure 6, the SML index rapidly intensified from -815 nT at 10:59 UT to -1073 nT at 11:03 UT. This is indicative of rapid enhancement of auroral activity and agrees with AE index response in Figure S3 of the supplementary material (Ngwira et al., 2023). Additionally, we also observe that the localization is wedged between the downward (blue) and upward (red) current amplitudes, which are a proxy for field-aligned currents (Weygand et al., 2011). This is consistent with findings from some earlier studies (Ngwira et al., 2018; Weygand, 2020).

4 Conclusions

Space weather is a natural hazard that can adversely impact some of the technological assets we rely on, such as the electric power transmission grids, which make up one of the most critical technological systems critical for national security and the economy. A major challenge pertaining to the study of GICs over the continental United States has been the access to GIC measurements. For the first time, this paper extensively investigates the occurrence of GICs greater than 10 A across the continental United States using measured GIC data from the EPRI SUNBURST project along with geomagnetic data from USGS and NRCan Observatory stations. Monitoring of GICs provides vital information to identify when and at what level GIC activity occurs. In the absence of this information, operations are based only on forecasting of solar activity along with real–time magnetometer information, and these values do not provide detailed information on GICs during GMD events. The investigation has revealed that:

- The number of GIC events recorded is well correlated with GMD activity with Kp index greater than 6 value. This is a firmly established observable trend that is expected since space weather is the key driver of geomagnetic variations that initiate the production of GICs.
- About 76% of top 17 GIC events that were investigated closely were attributed to the storm main phase, while only 24% were associated with storm sudden commencements. It should be emphasized here that these results are only valid for GIC events presented in Table 2 and not representative of the entire data set. ~~The other events in the GIC dataset need to be further investigated as well in future. However, that is out of the scope of this study.~~The other events in the GIC dataset will be investigated further in a more comprehensive planned future study.
- For the first time, this study provides direct evidence showing that mid-latitude positive bays (MPBs) can drive large GIC events. MPBs are commonly associated with auroral substorm-related activity. Their ability to possibly cause severe GICs has been discussed in previous studies, but no direct evidence ever offered.
- This study also shows that the largest measured GIC event in the dataset was associated with a localized intense dB/dt structure sometimes called "geomagnetic hot spots" that was attributed to substorm-related activity. Again, to the best of the authors knowledge, this is the first time that a localized dB/dt "hot spot" is directly linked to production of large GICs.

- ~~Finally, some GIC events are not well correlated with dB/dt variations, therefore, a more details treatment of individual GIC events is suggested for a better understanding of their production and the coupling of space weather to the power grid.~~ Finally, access to more critical information about the transformers and the power grid is required for a full detailed analysis of the GIC events. The limitation is that investigators may need to have specific agreements with power utility operators to again access to that information. Therefore, an interdisciplinary collaborative approach involving players from the science community and power utilities is recommended.

Open Research

The solar wind data used in this study were obtained from the NASA/GSFC Space Physics Data Facility OMNIWeb service at `https://omniweb.gsfc.nasa.gov/`. The SuperMag SML index is derived from data collected at ground magnetometer stations around the world and made available at `http://supermag.jhuapl.edu/indices/`. The GIC data used in this study was made available via the CUA-EPRI partnership, however, the data is also accessible to the general public through the NERC GMD website (`https://www.nerc.com/pa/RAPA/GMD/Pages/GMDHome.aspx`).

Acknowledgments

This work was supported by NASA Grant Award 80NSSC20K1364 under the SWO2R program. The authors gratefully acknowledge NASA/GSFC Space Physics Data Facility service for solar wind and geomagnetic AE/Sym-H index data used in this study (`https://omniweb.gsfc.nasa.gov/`). The results presented in this paper rely on data collected at magnetic observatories. We thank the national institutes that support them and INTERMAGNET for promoting high standards of magnetic observatory practice (`www.intermagnet.org`). The authors also thank the personnel and institutes that are associated with the global magnetometer networks that contribute data to SuperMag (`http://supermag.jhuapl.edu/mag`). SuperMAG is funded by NSF, NASA and ESA.

References

Akasofu, S.-I. (2018). A review of the current understanding in the study of geomagnetic storms. *International Journal of Earth Science and Geophysics*, *4*, 2631-5033.

Amm, O. (1997). Ionospheric elementary current systems in spherical coordinates and their application. *Journal of Geomagnetism and Geoelectricity*, *49*(7), 947–955.

Bernabeu, E. E. (2013). Modeling Geomagnetically Induced Currents in the Dominion Virginia Power Using Extreme 100-Year Geoelectric Field Scenarios – Part 1. *IEEE Transactions on Power Delivery*, *28*, 516-523.

Blake, S. P., Pulkkinen, A., Schuck, P. W., Glocer, A., Oliveira, D. M., Welling, D. T., ... Quaresima, G. (2021). Recreating the Horizontal Magnetic Field at Colaba During the Carrington Event With Geospace Simulations. *Space Weather*, *19*. doi: 10.1029/2020SW002585

Blandin, M., Connor, H. K., Öztürk, D. S., Keesee, A. M., Pinto, V. A., Mahmud, M. S., ... Priyadarshi, S. (2022). Multi-Variate LSTM Prediction of Alaska Magnetometer Chain Utilizing a Coupled Model Approach. *Frontiers in Astronomy and Space Sciences*. doi: 10.3389/fspas.2022.846291

Bolduc, L. (2002). GIC Observations and Studies in the Hydro-Québec Power System. *Journal of Atmospheric and Solar Terrestrial Physics*, *64*(16), 1793–1802.

Boteler, D. H. (2001). Space Weather Effects on Power Systems. *In Song D., Singer H.J and Siscoe G.L. Space Weather. AGU Geophysical Monograph 125*,

347–352.
Boteler, D. H. (2019). A 21st Century View of the March 1989 Magnetic Storm. *Space Weather*, *17*. doi: 10.1029/2019SW002278
Chu, X., McPherron, R. L., Hsu, T. S., & Angelopoulos, V. (2015). Solar Cycle Dependence of Substorm Occurrence and Duration: Implications for Onset. *Journal of Geophysical Research*, *120*, 2808–2818. doi: 10.1002/2015JA021104
Dimmock, A. P., Rosenqvist, L., Welling, D. T., Viljanen, A., Honkonen, I., Boynton, R. J., & Yordanova, E. (2020). On the Regional Variability of dB/dt and Its Significance to GIC. *Space Weather*, *18*. doi: 10.1029/2020SW002497
Engebretson, M. J., Pilipenko, V. A., Steinmetz, E. S., Moldwin, M. B., Connors, M. G., Boteler, D. H., … Russell, C. T. (2021). Nighttime Magnetic Perturbation Events Observed in Arctic Canada: 3. Occurrence and Amplitude as Functions of Magnetic Latitude, Local Time, and Magnetic Disturbance Indices. *Space Weather*, *19*. doi: https://doi.org/10.1029/2020SW002526
EPRI. (2008). *Monitoring and Mitigation of Geomagnetically Induced Currents, EPRI, Palo Alto, CA: 2008.1015938.*
EPRI. (2020). *Use of Magnetotelluric Measurement Data to Validate/Improve Existing Earth Conductivity Models, EPRI, Palo Alto, CA: 2020.3003019425.*
EPRI. (2022). *B2ECalc: Geoelectric Field Computation Tool Version 1.0., EPRI, Palo Alto, CA: 2022. 3002024617. www.epri.com/research/products/000000003002024617.*
Federal Energy Regulatory Commission. (2015). *Reliability Standard for Transmission System Planned Performance for Geomagnetic Disturbance Events, 18 CFR Part 40, Docket No. RM15-11-000.*
Gritsutenko, S., Korovkin, N., Sakharov, Y., & Sokolova, O. (2023). Assessment of Geomagnetically Induced Currents Impact on Power Grid Modelling. *Magnetism*, *3*(2), 135–147. doi: 10.3390/magnetism3020011
Guerrero, A., Palacios, J., Rodríguez-Bouza, M., Rodríguez-Bilbao, I., Aran, A., Cid, C., … Cerrato, Y. (2017). Storm and Substorm Causes and Effects of Midlatitude Location for St. Patricks's 2013 and 2015 Events. *Journal of Geophysical Research*, *122*. doi: 10.1002/2017JA024224
Horton, R., Boteler, D., Overbye, T. J., Pirjola, R., & Dugan, R. C. (2012). A Test Case for the Calculation of Geomagnetically Induced Currents. *IEEE Transactions on Power Delivery*, *27*, 2368-2373.
Kappenman, J. G. (2003). Storm Sudden Commencement Events and the Associated Geomagnetically Induced Current Risks to Ground-based Systems at Low-latitude and Midlatitude Locations. *Space Weather*, *1*. doi: 10.1029/2003SW000009
Keesee, A. M., Pinto, V. A., Coughlan, M., Lennox, C., Mahmud, M. S., & Connor, H. K. (2020). Comparison of Deep Learning Techniques to Model Connections Between Solar Wind and Ground Magnetic Perturbations. *Frontiers in Astronomy and Space Sciences*. doi: 10.3389/fspas.2020.550874
Kelbert, A. (2020). EMTF XML: New Data Interchange Format and Conversion Tools for Electromagnetic Transfer Functions. *Geophysics*, *85*. doi: https://doi.org/10.1190/geo2018-0679.1
Kelbert, A., Balch, C. C., Pulkkinen, A., Egbert, G. D., Love, J. J., Rigler, E. J., & Fujii, I. (2017). Methodology for Time-domain Estimation of Storm Time Geoelectric Fields Using the 3-D Magnetotelluric Response Tensors. *Space Weather*, *15*. doi: 10.1002/2017SW001594
Kelbert, A., Erofeeva, S., Trabant, C., Karstens, R., Fossen, M. V., Egbert, G., & Schultz, A. (2011). IRIS DMC Data Services Products: EMTF, The Magnetotelluric Transfer Functions. *U.S. Geological Survey*. doi: https://doi.org/10.17611/DP/EMTF.1
Kepko, L., McPherron, R. L., Amm, O., Apatenkov, S., Baumjohann, W., Birn, J., … Sergeev, V. (2015). Substorm Current Wedge Revisited. *Space Science*

Reviews, *190*, 1–46. doi: https://doi.org/10.1007/s11214-014-0124-9

Kikuchi, T., & Araki, T. (1979). Horizontal Transmission of the Polar Electric Field. *Journal of Atmospheric and Terrestrial Physics*, *41*, 927–936.

Lesher, R., Porter, J., & Byerly, R. (1994). SUNBURST – a Network of GIC Monitoring Systems. *IEEE Transactions on Power Delivery*, *9*(1), 128-137. doi: 10.1109/61.277687

Lewis, Z. M., Wild, J. A., Allcock, M., & Walach, M.-T. (2022). Assessing the impact of weak and moderate geomagnetic storms on uk power station transformers. *Space Weather*, *20*(4), e2021SW003021. doi: https://doi.org/10.1029/2021SW003021

Lucas, G. M., Love, J. J., Kelbert, A., Bedrosian, P. A., , & Rigler, E. J. (2020). A 100-year Geoelectric Hazard Analysis for the U.S. High-Voltage Power Grid. *Space Weather*, *18*. doi: 10.1029/2019SW002329

McPherron, R. L., & Chu, X. (2017). The Mid-latitude Positive Bay and the MPB Index of Substorm Activity. *Space Science Reviews*, *206*, 91–122. doi: 10.1007/s11214-016-0316-6

McPherron, R. L., & Chu, X. (2018). The Midlatitude Positive Bay Index and the Statistics of Substorm Occurrence. *Journal of Geophysical Research*, *123*, 2831–2850. doi: 1002/2017JA024766

Moodley, N., & Gaunt, C. T. (2017). Low Energy Degradation Triangle for power transformer health assessment. *IEEE Transactions on Dielectrics and Electrical Insulation*, *24*(1), 639-646. doi: 10.1109/TDEI.2016.006042

Newell, P. T., & Gjerloev, J. W. (2011). Evaluation of SuperMAG auroral electrojet indices as indicators of substorms and auroral power. *Journal of Geophysical Research*, *116*, A12211. doi: 10.1029/2011JA016779

Ngwira, C. M., Arritt, B., Perry, C., Weygand, J. M., & Sharma, R. (2023). Occurrence of Large Geomagnetically Induced Currents Within the EPRI SUNBURST Network: Supplemental Materials. *Dryad, Dataset*. doi: https://doi.org/10.5061/dryad.sf7m0cgc6

Ngwira, C. M., Pulkkinen, A., Bernabeu, E., Eichner, J., Viljanen, A., & Crowley, G. (2015). Characteristics of Extreme Geoelectric Fields and Their Possible Causes: Localized Peak Enhancements. *Geophysical Research Letters*, *42*. doi: 10.1002/2015GL065061

Ngwira, C. M., Pulkkinen, A., Kuznetsova, M. M., & Glocer, A. (2014). Modeling Extreme 'Carrington–type' Space Weather Events Using Three-dimensional MHD Code Simulations. *Journal of Geophysical Research*, *119*. doi: 10.1002/2013JA019661

Ngwira, C. M., Pulkkinen, A., Wilder, F. D., & Crowley, G. (2013). Extended Study of Extreme Geoelectric Field Event Scenarios for Geomagnetically Induced Current Applications. *Space Weather*, *11*. doi: 10.1002/swe.20021

Ngwira, C. M., Sibeck, D., Silveria, M. V. D., Georgiou, M., Weygand, J. M., Nishimura, Y., & Hampton, D. (2018). A Study of Intense Local dB/dt Variations During two Geomagnetic Storms. *Space Weather*, *16*. doi: 10.1029/2018SW001911

Nishimura, Y., Lyons, L., Gabrielse, C., Weygand, J. M., Donovan, E. F., & Angelopoulos, V. (2020). Relative Contributions of Large-scale and Wedgelet Currents in the Substorm Current Wedge. *Journal of Geophysical Research*, *72*. doi: 10.1186/s40623-020-01234-x

North American Electric Reliability Corporation. (1989). *1989 NERC Hydro Quebec GMD Event Report.*

Oliveira, D. M., Arel, D., Raeder, J., Zesta, E., Ngwira, C. M., Carter, B. A., ... Gjerloev, J. W. (2018). Geomagnetically Induced Currents Caused by Interplanetary Shocks with Different Impact Angles and Speeds. *Space Weather*, *16*, 636–647. doi: 10.1029/2018SW001880

Oliveira, D. M., & Raeder, J. (2014). Impact Angle Control of Interplane-

tary Shock Geoeffectiveness. *Journal of Geophysical Research*, *119*. doi: 10.1002/2014JA020275
Oliveira, D. M., Weygand, J. M., Zesta, E., Ngwira, C. M., Hartinger, M. D., Xu, Z., . . . Souza, V. M. (2021). Impact Angle Control of Local Intense dB/dt Variations During Shock-Induced Substorms. *Space Weather*, *19*. doi: 10.1029/2021SW002933
Overbye, T. J., Shetye, K. S., Hutchins, T. R., Qiu, Q., & Weber, J. D. (2013). Power Grid Sensitivity Analysis of Geomagnetically Induced Currents. *IEEE Transactions on Power Systems*, *28*(4). doi: 10.1109/TPWRS.2013.2274624
Oyedokun, D. (2015). *Geomagnetically Induced Currents (GIC) in Large Power Systems Including Transformer Time Response* (Unpublished doctoral dissertation). University of Cape Town, Faculty of Engineering the Built Environment, Department of Electrical Engineering. (Available from: http://hdl.handle.net/11427/16708)
Oyedokun, D., Heyns, M., Cilliers, P., & Gaunt, C. T. (2020). Frequency Components of Geomagnetically Induced Currents for Power System Modelling. *International SAUPEC/RobMech/PRASA Conference*. doi: 10.1109/SAUPEC/RobMech/PRASA48453.2020.9041021
Pinto, V. A., Keesee, A. M., Coughlan, M., Mukundan, R., Johnson, J. W., Ngwira, C. M., & Connor, H. K. (2022). Field-Aligned Current Observations using the DICE Body Mounted Magnetometer. *Frontiers in Astronomy and Space Sciences*. doi: 10.3389/fspas.2022.869740
Pirjola, R. (2000). Geomagnetically Induced Currents During Magnetic Storms. *IEEE Trans. Plasma Sci.*, *28*(6), 1867-1873.
Pulkkinen, A., Bernabeu, E., Eichner, J., Viljanen, A., & Ngwira, C. M. (2015). Regional-scale High-latitude Extreme Geoelectric Fields Pertaining to Geomagnetically Induced Currents. *Earth, Planets and Space*, *67*. doi: 10.1186/s40623-015-0255-6
Pulkkinen, A., Bernabeu, E., Thomson, A., Viljanen, A., Pirjola, R., Boteler, D., . . . MacAlester, M. (2017). Geomagnetically Induced Currents: Science, Engineering and Applications Readiness. *Space Weather*, *15*. doi: 10.1002/2016SW001501
Rezaei-Zare, A., Marti, L., Narang, A., & Yan, A. (2016). Analysis of Three-Phase Transformer Response due to GIC Using an Advanced Duality-Based Model. *IEEE Transactions on Power Systems*, *31*(5). doi: 10.1109/TPWRD.2015.2505499
Schillings, A., Palin, L., Opgenoorth, H. J., Hamrin, M., Rosenqvist, L., Gjerloev, J. W., . . . Barnes, R. (2022). Distribution and Occurrence Frequency of dB/dt Spikes During Magnetic Storms 1980–2020. *Space Weather*, *20*. doi: 10.1029/2021SW002953
Schultz, A. (2009). EMScope: A Continental Scale Magnetotelluric Observatory and Data Discovery Resource. *Data Science Journal*, *8*.
Smith, A. W., Freeman, M. P., Rae, I. J., & Forsyth, C. (2019). The influence of Sudden Commencements on the Rate of Change of the Surface Horizontal Magnetic Field in the United Kingdom. *Space Weather*, *17*. doi: 10.1029/2019SW002281
Tsurutani, B. T., & Hajra, R. (2023). Energetics of Shock-triggered Supersubstorms (SML < -2500 nT). *The Astrophysical Journal*, *946*. doi: 10.3847/1538-4357/acb143
Tsurutani, B. T., Lakina, G. S., Verkhoglyadova, O. P., Gonzalez, W. D., Echer, E., & Guarnieri, F. L. (2011). A Review of Interplanetary Discontinuities and Their Geomagnetic Effects. *Journal of Atmospheric and Solar Terrestrial Physics*, *73*, 5–19.
Villante, U., & Piersanti, M. (2011). Sudden Impulses at Geosynchronous Orbit and at Ground. *Journal of Atmospheric and Solar-Terrestrial Physics*, *73*. doi: 10

.1016/j.jastp.2010.01.008
Welling, D. T., Love, J. J., Rigler, E. J., Oliveira, D. M., & Komar, C. M. (2020). Numerical Simulations of the Geospace Response to the Arrival of a Perfect Interplanetary Coronal Mass Ejection. *Space Weather*, *19*. doi: 10.1029/2020SW002489
Weygand, J. M. (2020). The Temporal and Spatial Development of dB/dt for substorms. *AIMS Geosciences*, *7(1)*, 74-94. doi: 10.3934/geosci.2021004
Weygand, J. M., Amm, O., Angelopoulos, V., Milan, S. E., Grocott, A., Gleisner, H., & Stolle, C. (2012). Comparison Between SuperDARN Flow Vectors and Equivalent Ionospheric Currents From Ground Magnetometer Arrays. *Journal of Geophysical Research*, *117*. doi: 10.1029/2011JA017407
Weygand, J. M., Amm, O., Viljanen, A., Angelopoulos, V., Murr, D., Engebretson, M. J., ... Mann, I. (2011). Application and Validation of the Spherical Elementary Currents Systems Technique for Deriving Ionospheric Equivalent Currents with the North American and Greenland Ground Magnetometer Arrays. *Journal of Geophysical Research*, *116*. doi: 10.1029/2010JA016177
Weygand, J. M., Engebretson, M. J., Pilipenko, V. A., Steinmetz, E. S., Moldwin, M. B., Connors, M. G., ... Gjerloev, J. (2016). SECS Analysis of Nighttime Magnetic Perturbation Events Observed in Arctic Canada. *Journal of Geophysical Research*, *126*. doi: https://doi.org/10.1029/2021JA029839
Weygand, J. M., Ngwira, C. M., & Arritt, R. F. (2023). The Equatorward Boundary of the Auroral Current System During Magnetic Storms. *Journal of Geophysical Research*, *128*, e2023JA031510. doi: https://doi.org/10.1029/2023JA031510
Yue, C., Song, Q. G., Zhang, H., Wang, Y. F., Yuan, C. J., Pu, Z. Y., ... Wang, C. R. (2010). Geomagnetic Activity Triggered by Interplanetary Shocks. *Journal of Geophysical Research*, *115*. doi: 10.1029/2010JA015356